

STABILIZING EFFECT OF MAGNETIC HELICITY ON MAGNETIC CAVITIES IN THE INTERGALACTIC MEDIUM

SIMON CANDELAESI

Division of Mathematics, University of Dundee, Dundee DD1 4HN, United Kingdom and
School of Mathematics and Statistics, University of Glasgow, Glasgow G12 8QQ, United Kingdom
simon.candelaesi@gmail.com

FABIO DEL SORDO

Institute of Astrophysics, FORTH, GR-71110 Heraklion, Greece and
Department of Physics, University of Crete, GR-70013 Heraklion, Greece
fabiods@ia.forth.gr*Draft version January 1, 2020*

ABSTRACT

We investigate the effect of magnetic helicity on the stability of buoyant magnetic cavities as found in the intergalactic medium. In these cavities we insert helical magnetic fields and test whether or not helicity can increase their stability to shredding through the Kelvin-Helmholtz instability and, with that, their life time. This is compared to the case of an external vertical magnetic field which is known to reduce the growth rate of the Kelvin-Helmholtz instability. By comparing a low-helicity configuration with a high helicity one with the same magnetic energy we find that an internal helical magnetic field stabilizes the cavity. This effect increases as we increase the helicity content. Stabilizing the cavity with an external magnetic field requires instead a significantly stronger field at higher magnetic energy. We conclude that the presence of helical magnetic fields is a viable mechanism to explain the stability of intergalactic cavities on time scales longer than 100 Myr.

Subject headings: intergalactic medium, magnetic helicity, hydromagnetic stability

1. INTRODUCTION

Intergalactic hot cavities have been observed to emanate from galactic disks in clusters of galaxies (e.g. Carilli et al. (1994); Carilli & Taylor (2002); Taylor et al. (2002); Churazov et al. (2001); Bîrzan et al. (2004); McNamara & Nulsen (2007); Montmerle (2011)). Similar but different structures have been observed also around our Galaxy, they are named Fermi Bubbles (Su et al. 2010) and their formation mechanism is still elusive (Yang et al. 2018). Observations seem to indicate that such intergalactic structures form as consequences of radio jets emanated by supermassive black holes or by active galactic nuclei (AGN) and their interaction with extragalactic plasma. These AGN-inflated radio bubbles in the intergalactic medium are seen in X-ray images of galaxy clusters. A shock is produced as the jet penetrates the surrounding medium, and, in order to achieve pressure equilibrium, the jet material expands leading to the formation of a low-density cavity. Bubbles at 10 kpc from the galactic center are found to be at least a factor of 3 less dense than the surrounding medium.

These hot cavities propagate through the intergalactic medium where they are subject to magnetohydrodynamical instabilities, such as the Rayleigh-Taylor instability, the Richtmyer-Meshkov instability, and in particular the Kelvin-Helmholtz (KH) instability, after which turbulent mixing occurs. However, estimates of their life time using their terminal velocity (e.g. Bîrzan et al. (2004)) suggests that they survive significantly longer than they should (of the order of 10 Myr-100 Myr).

The intergalactic medium can be modeled as high-conductivity plasma. Chandrasekhar (1961); Sharma & Srivastava (1968) showed analytically how in the presence of a magnetic field parallel to the velocity the KH instability is suppressed. However, a perpendicular field has no effect on the growth of the modes. The effect of an

external magnetic field on the stability of the cavities has been subject of several studies (e.g. Robinson et al. 2004). However, the interiors of these cavities may be magnetized too. This is possible, for instance, if the jet responsible for their inflation is magnetized. Also, there is the possibility that the turbulent motions arising during the generation of the cavities may amplify the magnetic field in its interior through e.g. a dynamo effect. The hypothesis of a helical magnetic field lying inside these bubbles appears justified also in light of results showing that AGN jets are characterized by helical magnetic fields (Li et al. 2006; Tang 2008; Gabuzda 2018). If this field contains magnetic helicity, it is stable on diffusive times, i.e. the energy and topology change insignificantly during this period (e.g., Del Sordo et al. 2010; Candelaesi & Brandenburg 2011).

If such an internal field was not stretched throughout the cavity boundaries where the KH instability occurs, it would have no immediate effect on the instability and we would not see a direct suppression of it. However, as the instability grows and leaves the linear regime, it can potentially be anyway suppressed at this later stage.

Intergalactic cavities have been simulated in the past and different effects were considered in order to understand their evolution and stability. For instance, Brüggén (2003) studied the cooling behavior in buoyant bubbles in galactic clusters, where there is a significant growth of the KH instability. Braithwaite (2010) studied the magnetohydrodynamic relaxation of AGN ejecta, finding that the time scale on which the bubble reaches an equilibrium depends on the magnetization and the helicity of the outflow. It should be noted however, that this study did not include the effect of buoyancy. Subsequently, Gourgoullos et al. (2010) studied the problem with both analytical and numerical approaches, finding that the presence of both poloidal and toroidal components of the magnetic field in intergalactic cavities does needed induce

stability. Liu et al. (2008) showed how the ratio of the toroidal to poloidal magnetic field of the bubble determines the direction of bubble expansion and propagation, which can develop asymmetries about its propagation axis. Dong & Stone (2009) studied the effect of magnetic fields and anisotropic viscosity, finding that a critical role for the evolution of the bubble is played by the initial field geometry, and that toroidal field loops initially located inside the bubble are the best option to reproduce the observed cavity structures.

Vogt & Enßlin (2005) observed how the typical length scale of magnetic fields in the Hydra A cluster is smaller than the typical bubble size, therefore concluding that the scenario of an uniform external field is not supported. Based on this result, Ruszkowski et al. (2007) studied the effect of a random magnetic field, taking into account both the helical and non-helical cases. They argued that when the gas pressure is higher than the magnetic pressure, that is for high plasma β (~ 40 in their case), a random helical magnetic field cannot stabilize the bubble. Still, they could not exclude that stabilization is taking place if plasma β is lower locally inside the intergalactic cavities. On the other hand, Jones & De Young (2005) found with 2D simulations that micro Gauss magnetic fields can stabilize these bubbles. In general, the evolution of the helicity of extragalactic bubbles and its interaction with the intergalactic medium, after the bubble's inflation and detachment from the jet, have been only marginally studied and they are not yet well understood, especially in three dimensions. Therefore, further investigation is needed, and the research we here present intends to be a step in this direction.

The aim of this work is to investigate the stabilizing effects of internal helical magnetic fields on the intergalactic cavities where they may be harbored. Moreover, we aim at comparing their stabilizing effect to that of a homogeneous external vertical field to evaluate whether a similar stabilizing effect may be attained with weaker fields. This work is organized as follows: In Section 2 we illustrate the model we implemented; In Section 3 we depict the effect of an internal helical magnetic field; In Section 4 we show the effect of an external magnetic field; and in Section 5 we draw some conclusions and implications of this work.

2. MODEL

Our model set-up consists of a hot under-dense bubble embedded in a stably stratified medium with gravity. This bubble rises through buoyancy, which leads to shear with the surrounding stationary medium and the onset of the Kelvin–Helmholtz instability on the bubble's surface. Our goal is to study how the stability of the bubble depends on the presence of magnetic fields. Therefore, concerning the stability of the bubbles we will consider three cases: (i) purely hydrodynamical case, (ii) internal helical magnetic field and (iii) external vertical magnetic field. The last scenario has already been studied for the Kelvin–Helmholtz instability for incompressible and compressible media by Chandrasekhar (1961) and here we will use it as reference. Cases (ii) and (iii) will be further subdivided into a high-helicity and low-helicity case and strong and weak external field case.

2.1. Governing equations

To approach this problem and to provide a quantitative assessment we make use of direct numerical simulations, that we perform with the public code Pencil Code (<https://github.com/pencil-code>). This code is particularly suitable for our study since it avoids using the

magnetic field \mathbf{B} as primary variable and instead uses its vector potential \mathbf{A} , hence ensuring the fields stay solenoidal throughout the simulations. Moreover it allows to quantify the magnetic helicity $H = \int \mathbf{A} \cdot \mathbf{B} dV$, where the integral is calculated over the whole computational domain. For our study we require an ideally conducting viscous medium. This is governed by the resistive magnetohydrodynamics equation together with the energy (temperature) equation:

$$\frac{\partial \mathbf{A}}{\partial t} = \mathbf{u} \times \mathbf{B} + \eta \nabla^2 \mathbf{A}, \quad (1)$$

$$\frac{D\mathbf{u}}{Dt} = -c_s^2 \nabla \left(\frac{\ln T}{\gamma} + \ln \rho \right) + \frac{\mathbf{J} \times \mathbf{B}}{\rho} - \mathbf{g} + \mathbf{F}_{\text{visc}}, \quad (2)$$

$$\frac{D \ln \rho}{Dt} = -\nabla \cdot \mathbf{u}, \quad (3)$$

$$\begin{aligned} \frac{\partial \ln T}{\partial t} = & -\mathbf{u} \cdot \nabla \ln T - (\gamma - 1) \nabla \cdot \mathbf{u} \\ & + \frac{1}{\rho c_v T} (\nabla \cdot (K \nabla T) + \eta \mathbf{J}^2 \\ & + 2\rho \nu \mathbf{S} \otimes \mathbf{S} + \zeta \rho (\nabla \cdot \mathbf{u})^2), \end{aligned} \quad (4)$$

with the magnetic vector potential \mathbf{A} , magnetic field $\mathbf{B} = \nabla \times \mathbf{A}$, fluid velocity \mathbf{u} , constant magnetic resistivity (diffusivity) η , advective derivative $D/Dt = \partial/\partial t + \mathbf{u} \cdot \nabla$, sound speed $c_s = \gamma p/\rho$, adiabatic index $\gamma = c_p/c_v$, heat capacities c_p and c_v at constant pressure and volume, temperature T , density ρ , electric current density $\mathbf{J} = \nabla \times \mathbf{B}$, gravitational acceleration \mathbf{g} , viscous force \mathbf{F}_{visc} , heat conductivity K and the bulk viscosity ζ . The viscous force is given as $\mathbf{F}_{\text{visc}} = \rho^{-1} \nabla \cdot 2\nu \rho \mathbf{S}$, with the traceless rate of strain tensor $S_{ij} = \frac{1}{2}(u_{i,j} + u_{j,i}) - \frac{1}{3}\delta_{ij} \nabla \cdot \mathbf{u}$. The equation of state used here is for the ideal monatomic gas and it appears implicitly in our equations, as we eliminated pressure p . Here the gas is monatomic with $\gamma = 5/3$.

Our side boundaries (xy) are chosen to be periodic, while the bottom is closed ($\mathbf{u} \cdot \mathbf{n} = 0$) and the top open. This allows for fluxes outwards. For the magnetic field the vertical boundaries are set to open, allowing for magnetic flux.

In order to reduce resistive magnetic helicity decay we choose a value of the magnetic resistivity as low as the resolution allows. Here we set it to $\eta = 3 \times 10^{-4}$. Viscosity is set to $\nu = 1 \times 10^{-3}$ for most simulations and to $\nu = 2 \times 10^{-4}$ for two comparisons, which prevents any accumulation of turbulent energy at small scales.

With the viscosity and magnetic resistivity we can then compute our Reynolds numbers:

$$\text{Re} = \frac{u_{\text{max}} d}{\nu} \quad (5)$$

$$\text{Re}_M = \frac{u_{\text{max}} d}{\eta}, \quad (6)$$

with the maximum velocity u_{max} and bubble diameter $d = 1.6$.

2.2. Initial condition

As initial condition we choose a stably stratified atmosphere in which we place an under-dense hot cavity of spherical shape. The stable atmosphere obeys the hydrostatic equilibrium

$$\rho \mathbf{g} = -\nabla p, \quad (7)$$

with the gravitational acceleration in negative z -direction g . Our model atmosphere extends in the z -direction which makes the gradient a derivative in z and we can rewrite equation (7) as

$$\rho g = -\frac{dp}{dz}. \quad (8)$$

Density, pressure and temperature are related through the ideal gas law

$$p = \frac{R}{\mu} \rho T, \quad (9)$$

where μ is the mass of one mol of gas and $R = 8.31 \text{ J K}^{-1} \text{ mol}^{-1}$ is the ideal gas constant. With the ideal gas law we can express the hydrostatic equilibrium as

$$\frac{\mu g}{R} \frac{dz}{T} = -\frac{dp}{p} \quad (10)$$

The gas is chosen to be adiabatic, i.e.

$$p^{1-\gamma} T^\gamma = \text{const.}, \quad (11)$$

which leads to the relation

$$\frac{dp}{p} = \frac{\gamma}{\gamma-1} \frac{dT}{T}. \quad (12)$$

With equation (10) we can write

$$\frac{dT}{dz} = -\frac{\gamma-1}{\gamma} \frac{\mu g}{R}. \quad (13)$$

We now integrate this equation and obtain

$$T = -\frac{\gamma-1}{\gamma} \frac{\mu g}{R} z + T_0, \quad (14)$$

where T_0 is the temperature at an arbitrary height z_0 .

We now choose this height to be the isothermal scale height

$$z_0 = \frac{RT_0}{\mu g}. \quad (15)$$

This is justified if we assume that the gas is in isothermal equilibrium at z_0 , which is a common assumption for the adiabatic atmosphere. Our temperature profile obtains now the form:

$$T(z) = T_0 \left(1 - \frac{\gamma-1}{\gamma} \frac{z}{z_0} \right). \quad (16)$$

With the temperature profile and equation (12) we can compute the pressure profile to

$$p(z) = p_0 \left(1 - \frac{\gamma-1}{\gamma} \frac{z}{z_0} \right)^{\gamma/(\gamma-1)}. \quad (17)$$

Taking equation (8) we can also compute the density profile to

$$\rho(z) = \rho_0 \left(1 - \frac{\gamma-1}{\gamma} \frac{z}{z_0} \right)^{1/(\gamma-1)}. \quad (18)$$

As simulation domain we choose a box of size 2.4×2.4 in the horizontal (xy) plane and 9.6 in the vertical (z), using $480 \times 480 \times 1920$ meshpoints. The cavity has a radius of 0.8 and is placed centrally in x and y and at 0.8 in z . Its initial temperature is $T_{\text{cavity}} = 4$ and density $\rho_{\text{cavity}} = 0.25$.

This should be contrasted to the surrounding medium which is stably stratified with gravitational acceleration of $g = 0.1$.

Model	$B(A_0)$	H_m	ν	η	k	Re	Re_M
hydro	-	-	10^{-3}	-	-	960	-
hydro2	-	-	2×10^{-4}	-	-	4800	-
hel_l	0.025	1	10^{-3}	3×10^{-4}	20	1280	4200
hel_h	0.1	4	10^{-3}	3×10^{-4}	5	1280	4200
hel_l2	0.025	1	2×10^{-4}	3×10^{-4}	20	5600	3700
hel_h2	0.1	4	2×10^{-4}	3×10^{-4}	5	6400	4200
ex_low	0.2	0	10^{-3}	3×10^{-4}	-	320	1000
ex_high	0.8	0	10^{-3}	3×10^{-4}	-	320	1000

TABLE 1

LIST OF SIMULATIONS WITH PARAMETERS USED IN THIS STUDY: THE MAGNETIC FIELD INTENSITY, MEASURED BY THE PARAMETER A_0 IN EQUATION (19), THE MAGNETIC HELICITY H_m , THE VISCOSITY ν , THE MAGNETIC DIFFUSIVITY η , THE PARAMETER k OF THE ABC FLOW IN EQUATION (19), THE REYNOLDS NUMBER Re AND THE MAGNETIC REYNOLDS NUMBER Re_M , AS DEFINED IN EQUATIONS (5) AND (6).

For that we choose $z_0 = 4$, $\rho_0 = 1$ and $T_0 = 1$ such that the cavity is in approximate pressure balance with its surrounding medium and its expansion or compression is insignificant.

For the magnetic case we insert a helical magnetic field of the Arnold-Beltrami-Childress (ABC) flow type:

$$\mathbf{A} = A_0 \begin{pmatrix} \cos((y - y_{\text{cavity}})k) + \sin((z - z_{\text{cavity}})k) \\ \cos((z - z_{\text{cavity}})k) + \sin((x - x_{\text{cavity}})k) \\ \cos((x - x_{\text{cavity}})k) + \sin((y - y_{\text{cavity}})k) \end{pmatrix}. \quad (19)$$

Taking the curl we obtain $\mathbf{B} = k\mathbf{A}$. The magnetic energy scales like $A_0^2 k^2$, while the magnetic helicity scales like $A_0^2 k$. By inversely scaling the amplitude A_0 and the inverse scale k we can change the magnetic helicity while keeping the magnetic energy fixed. For our low-helicity set up we choose $A_0 = 2.5 \times 10^{-2}$ and $k = 20$. For the high helicity case we choose $A_0 = 0.1$ and $k = 5$. For simplicity we will occasionally write $H = 1$ and $H = 4$ for the two cases.

2.3. Test Cases

As previously said, we consider three kinds of test cases. For a fair comparison, and a quantitative evaluation of the role of a magnetic field, we first perform calculations of a purely hydrodynamical case with no magnetic fields. We compare this with two cases with an internal magnetic field within the cavities. Both of them contain almost the same magnetic energy, while one has a topology that gives it a four times larger magnetic helicity. Finally, we take into account a third case, where an external magnetic field along the z direction is present during the ascent of the bubble. An overview over the parameters used in the simulations is show in Table 1. With these initial conditions we can compute the plasma β where the magnetic field is strongest using

$$\beta = \min \left(\frac{2(R\rho T/\mu)}{B^2} \right). \quad (20)$$

We compute this to be $\beta = 0.144$ for the helical cases. However, we have to notice that this is the minimum value β attains in our model since, with the presence of magnetic null points within the domain, β is not constant and even diverges at some points. In the external field cases we have instead $\beta = 0.9$ (weak field) and $\beta = 0.056$ (strong field).

2.4. Unit Conversions

We choose the conversion rate from code units to physical units such that the dimensions of the setups correspond to physically observed numbers in the intergalactic medium (see Table 2).

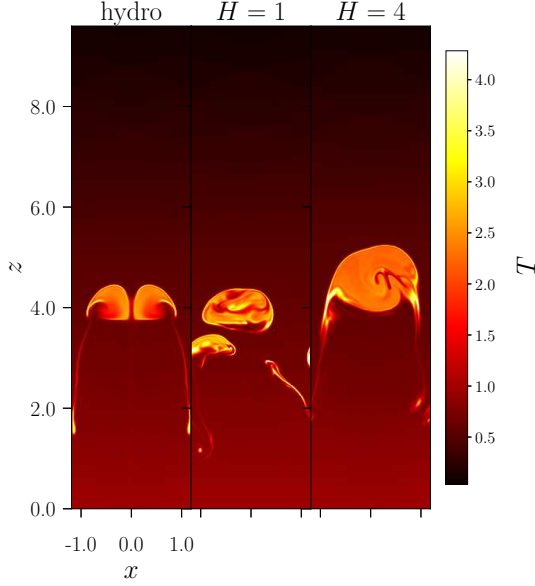


FIG. 1.— Slices through the simulation domain showing the temperature distribution at final times ($t = 20$) for the purely hydrodynamical case (left), weak helicity case (center) and strong helicity case (right) (models hydro, hel_l and hel_h in table Table 1).

one code unit of	physical unit
length	10 kpc
time	10 Myr
density	$10^{-25} \text{ g cm}^{-3}$
temperature	10^6 K
magnetic field	10^{-4} G

TABLE 2
CODE UNIT CONVERSION TABLE.

With these code unit conversions our set up has a size of $L_{xy} = 24 \text{ kpc}$ horizontally and $L_z = 96 \text{ kpc}$ vertically. The cavity has a radius of $r_b = 8 \text{ kpc}$ with a density of $\rho_b = 2.5 \times 10^{-26} \text{ g cm}^{-3}$ and temperature of $T_b = 4 \times 10^6 \text{ K}$. The surrounding medium at $z = 0$ has a density of $\rho_0 = 1 \times 10^{-25} \text{ g cm}^{-3}$ and temperature of $T_0 = 1 \times 10^6 \text{ K}$. On the system acts the gravitational acceleration of $g = 3.0985 \times 10^{-7} \text{ cm s}^{-2}$. Our simulations then run between 200 Myr and 250 Myr. The amplitude of the magnetic field is between $B_0 = 2.5 \times 10^{-6} \text{ G}$ and $B_0 = 1 \times 10^{-5} \text{ G}$. For the viscosity we obtain $\nu = 3.0172 \times 10^{27} \text{ cm}^2 \text{ s}^{-1}$ and resistivity $\eta = 9.0516 \times 10^{26} \text{ cm}^2 \text{ s}^{-1}$.

3. EFFECT OF AN INTERNAL HELICAL MAGNETIC FIELD

The first case we take into account is the the purely hydrodynamical one, to which we will compare the simulations including magnetic fields. As the cavity rises the Kelvin–Helmholtz instability acts on its interface with the surrounding medium and eventually affects the entire cavity by non-linear Kelvin–Helmholtz instability induced turbulent mixing, as illustrated in the left panel of Figure 1.

We then perform two different simulations including a helical magnetic field inside the cavity. There it becomes evident that magnetic helicity contributes to keep the cavity in a significantly more coherent state and prevents its disruption, provided a minimum amount of helicity is present in the field. This is evident from the central and left panels of Figure 1, showing two helical cases: the amount of magnetic helicity in

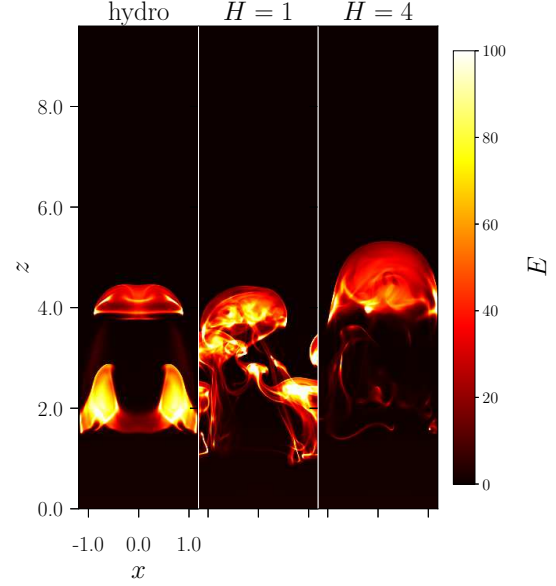


FIG. 2.— Emission measure at final times ($t = 20$) for the purely hydrodynamical case (left), weak helicity case (center) and strong helicity case (right).

the simulation shown in the right panel is 4 times larger than that in the central panel.

In order to make it easier to compare our results with observations we create artificial emission measures, assuming an optically thin medium. We place the observer along the y axis at an infinite distance. The emission measure E is then simply the line integral of the temperature to the fourth power

$$E(x, z) = \int T^4 dy. \quad (21)$$

Similar to the slices plotted in Figure 1, we observe from the emission measures (Figure 2) an increased stability when a helical magnetic field is present.

We can also observe this behavior in the volume rendering of the temperature (Figure 3). While the purely hydrodynamical case (left panel) and the low-helicity case (center) disintegrate after two bubble diameter crossings, the strongly helical case (right) remains largely intact. We can also observe that the purely hydrodynamical case is, as expected, symmetric about the central axis of the domain. Conversely, the disruption of the cavity in the low-helicity case develops a very asymmetric, chaotic structure. Also in the high-helicity case, although the disruption is only marginal, we can still observe an asymmetric evolution of the cavity.

To test the stability of the cavities we measure their coherence. In order to do so, we start by defining the space filled by the cavity as the loci for which $\log_{10}(T) > 1.5$. We choose this threshold because the surrounding cold medium has a significantly lower temperature and in the simulated times we do not observe a high enough temperature diffusion or conduction that would reduce the cavity temperature below this value. We then measure the mean distance d_{mean} of all the points in the cavity

$$d_{\text{mean}} = \langle |\mathbf{r}_{\text{cavity}} - \mathbf{r}_{\text{CM}}| \rangle, \quad (22)$$

where \mathbf{r}_{CM} is the position vector to the center of mass defined

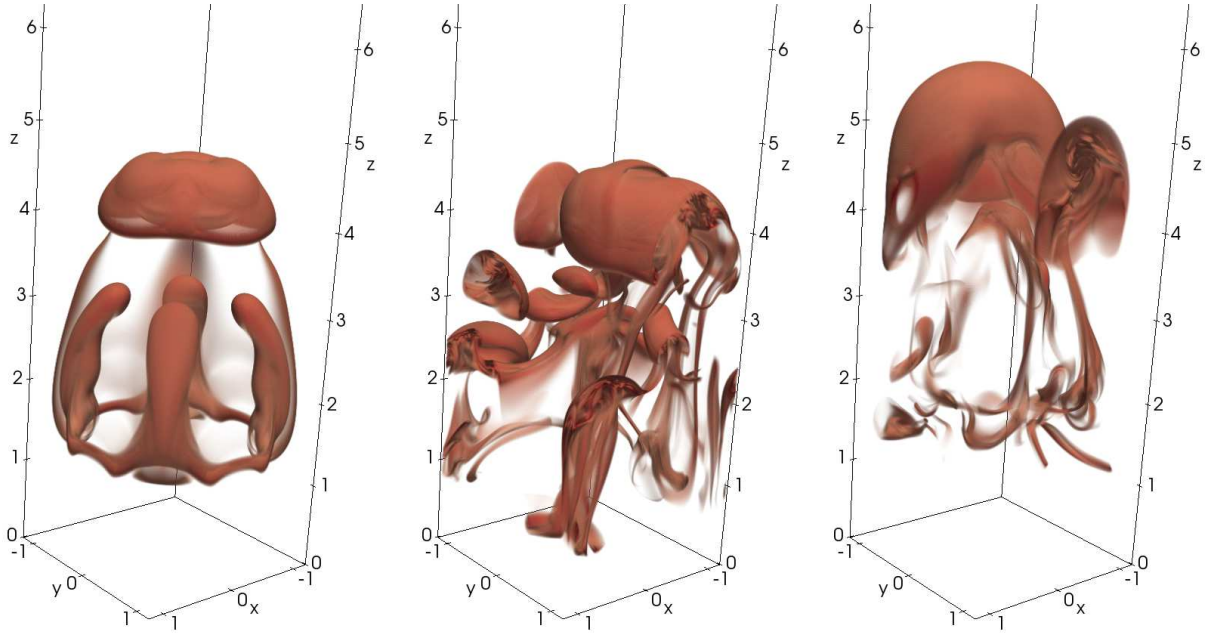


FIG. 3.— Volume rendering of the temperature of the magnetic cavity for the hydrodynamical case (left), low magnetic helicity (center) and high magnetic helicity (right) at $t = 20$. It is evident that magnetic helicity plays a role in determining the topology of the cavity. In particular, the symmetry seen in the hydrodynamical case is broken when magnetic helicity is non-zero.

as

$$\mathbf{r}_{\text{CM}} = \frac{\int_{\log_{10}(T) > 1.5} T \mathbf{r} dV}{\int_{\log_{10}(T) > 1.5} T dV}, \quad (23)$$

where $\mathbf{r}_{\text{cavity}}$ is the position vector to a point within the cavity, i.e. $\log_{10}(T) > 1.5$, and we take the average over the entire domain. We can therefore study the evolution of d_{mean} with time. Since some of the bubbles rise at different speeds, due to the different magnetohydrodynamic parameters of different models, we can also study the behavior of d_{mean} as function of the height reached by the bubble, i.e. by its center of mass. For that we also compute the mean height of the bubbles as

$$z_{\text{mean}} = \langle |z_{\text{cavity}} - z_{\text{CM}}| \rangle, \quad (24)$$

where we use the loci for which $\log_{10}(T) > 1.5$, similar as we do for d_{mean} .

Figure 4 depicts d_{mean} as function of z_{mean} in our simulations. We observe that without a magnetic field the cavity is dispersed without reaching far away from its starting position. An internal magnetic field with a low helicity content (model *hel_l1* in table Table 1) does not improve significantly the stability for almost the whole simulation, but it has a stabilizing effect towards the end. However, an internal field with higher magnetic helicity (model *hel_h1* in table Table 1), and the same magnetic energy has some clear positive effect on the bubble's stability. In this latter case we observe a relatively stable rise throughout. Figure 5 depicts instead the time evolution of d_{mean} . Here too it is evident how the strong-helical case is the most stable, whilst the low helical one only marginally stabilizes the cavity. From Figure 5 we can see that high helicity stabilizes the cavity for at least 250 Myr, whilst the hydrodynamical case and the low-helicity case disrupt after about 100 Myr.

3.1. Behavior at Higher Reynolds Number

We test the effect of a higher fluid Reynolds number on our results by performing simulations with a lower viscosity, $\nu =$

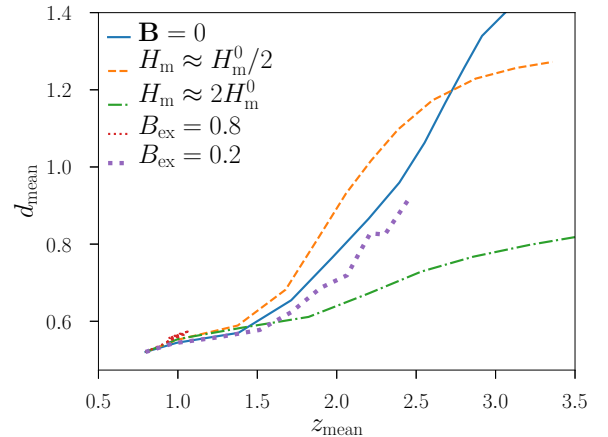


FIG. 4.— Coherence measure d_{mean} of the cavities in dependence of the mean height for the hydrodynamical, weak and strong-helicity case and weak and strong external field cases. We clearly observe that a large amount of magnetic helicity increases the cavities' stability. A comparable effect can only be obtained with a substantially stronger external magnetic field, but such a field inhibits the ascent of the bubble in the intergalactic medium.

2×10^{-4} for the hydrodynamical and the helical cases (models *hydro2*, *hel_l2*, and *hel_h2* in table Table 1). There we observe a clearer onset of the Kelvin–Helmholtz instability. However, the coherence measure does not change significantly for any of the models compared to the low Reynolds number case, and the relative behaviour between the hydrodynamical case and the two cases with internal helical magnetic fields resembles that obtained with higher viscosity (Figure 6). Therefore, this confirms our results in the lower Reynolds number regime.

4. EFFECT OF AN EXTERNAL PARALLEL MAGNETIC FIELD

From Chandrasekhar (1961) and Sharma & Srivastava (1968) we know that the Kelvin–Helmholtz instability is suppressed by a magnetic field that is aligned (parallel) to

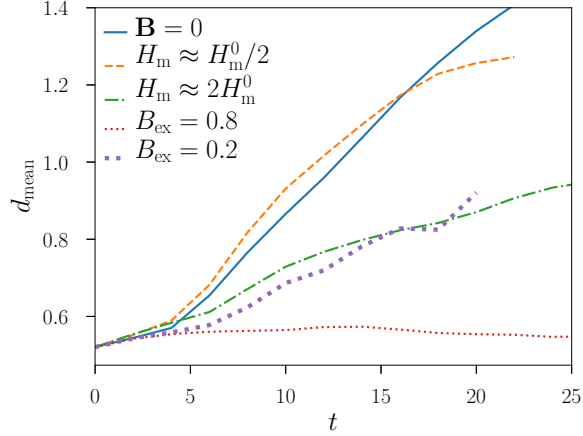


FIG. 5.— Coherence measure d_{mean} of the cavities in dependence of time for the hydrodynamical, weak and strong helicity case and weak and strong external field cases. The weak helicity case differs from the hydro case in the last part of the simulation. The strong helicity case shows a clear increase of the bubble stability, similar to that of an external parallel field. The case of very strong external parallel field keeps the bubble very stable, but it completely obstructs its ascent, hence keeping it confined in the lowest part of the domain. Note that the high helicity and strong external field simulations continue well beyond the plotted time limit.

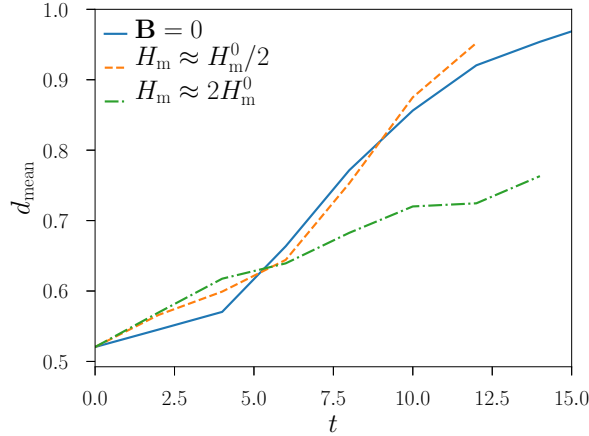


FIG. 6.— Coherence measure d_{mean} of the cavities for the high fluid Reynolds number cases in dependence of time for the hydrodynamical, weak and strong helicity case. The weak helicity case differs from the hydro case in the last part of the simulation. The strong helicity case shows a clear increase of the bubble stability, confirming our low Reynolds number results.

the velocity. Comparing equation (13) in chapter IV from Chandrasekhar (1961) with our induction equation (1) we observe that we can identify our \mathbf{B} with \mathbf{H} and the magnetic resistivity η has the same definition and the permeability $\mu = 1$ in our formulation.

With that we can write the equation (205) in chapter XI from Chandrasekhar (1961) as

$$B^2 \geq 2\pi(u_1 - u_2)^2(\rho_1\rho_2)/(\rho_1 + \rho_2), \quad (25)$$

which gives us a criterion for the Kelvin-Helmholtz instability to be entirely suppressed for a two-layer system with densities ρ_1 and ρ_2 and velocities u_1 and u_2 . For our hydrodynamic simulations we observe a velocity difference of ca. 0.5, while our densities are 1 (surrounding medium) and 0.25 (hot cavity). With that we estimate the magnetic field strength paral-

lel to the velocity to be ca. 0.56 for suppressing the Kelvin-Helmholtz instability.

Here we present the evolution of such a cavity with $\mathbf{B} = 0.8\mathbf{e}_z$ and one with $\mathbf{B} = 0.2\mathbf{e}_z$. That is, one will exhibit Kelvin-Helmholtz suppression at all scales, while the other will not. For a field that is strong enough for suppression we are in a situation with little buoyancy, that is z_{mean} remains approximately constant in time (Figure 4). It is worth noticing that both these cases with a magnetic field along \mathbf{e}_z have a total magnetic energy between one and two order of magnitude higher than the helical cases.

5. DISCUSSION AND CONCLUSIONS

In this work we have examined the possibility that an helical magnetic field may play a key role in the stability of extragalactic bubbles, similar to the Fermi bubbles observed raising from the midplane of our Galaxy in the intergalactic medium. This hypothesis appears justified, because these bubbles are thought to be inflated by AGN or from jets coming from the galactic center. Such jets have been observed to be characterized by helical magnetic fields, which is a consequence of the rotation of strong magnetic field from their sources. Since magnetic helicity is conserved in a high-conductivity medium, such as the intergalactic medium, it is reasonable to think the bubbles raising in the intergalactic medium to retain their helical magnetic field. As we used parameters that can be compared to measurements from the intergalactic medium we can directly draw an analogy between our simulations and observations.

For the purely hydrodynamical case we observe a longer stability (ca. 80 Myr) than has been predicted for bubbles in the intergalactic medium, although with an increase of ca. 50% in the coherence measure d_{mean} . While a parallel magnetic field is known to suppress the Kelvin-Helmholtz instability, for the case of intergalactic magnetic cavities the field strength would need to be rather large. Here we have shown that we can exploit the stability properties of magnetically helical structures to keep these cavities from disrupting, with a much smaller magnetic energy content.

We used a general helical magnetic field in the form of the ABC flow that fills a bubble raising through buoyancy in an otherwise stably stratified medium. We quantify the disruption of the bubble by measuring the parameter d_{mean} , the mean distance of all the points contained in it. We observed that this bubble is stabilized and does not develop a Kelvin-Helmholtz instability in the interface with the surrounding medium if the magnetic field is sufficiently helical. We estimated that a helical field with maximum strength of the order of 10^{-5} G can stabilize the bubble over a time scale of about 250 Myr. Here we see that during that time the high helicity case never exceeds a value of d_{mean} twice its initial value. Conversely, a less helical magnetic field, with a total magnetic helicity 4 times lower, cannot keep the bubble stable and this case exhibits a disruption similar to the non-magnetic case. In the low-helicity and hydrodynamic cases d_{mean} increases by more than twice its initial value. Therefore, based on the results here presented, we propose that an internal helical magnetic field is a viable explanation of intergalactic bubble stability, requiring only relatively low magnetic energies compared to the external magnetic field hypothesis.

ACKNOWLEDGMENTS

The authors appreciate the support given by the HPC3 Europe program HPC-EUROPA3 (INFRAIA-2016-1-730897).

SC acknowledges financial support from the UK's STFC (grant number ST/K000993). The authors thank Department of physics of the University of Crete for the hospitality and

Evangelia Ntormousi, Alexander Russell, David I. Pontin, Gunnar Hornig and Ross Palister for constructive and critical discussions.

REFERENCES

- Bîrzan, L., Rafferty, D. A., McNamara, B. R., Wise, M. W., & Nulsen, P. E. J. 2004, *Astrophys. J.*, 607, 800
- Braithwaite, J. 2010, *Mon. Not. R. Astron. Soc.*, 406, 705
- Brüggen, M. 2003, *Astrophys. J.*, 592, 839
- Candelaresi, S., & Brandenburg, A. 2011, *Phys. Rev. E*, 84, 016406
- Carilli, C. L., Perley, R. A., & Harris, D. E. 1994, *Mon. Not. R. Astron. Soc.*, 270, 173
- Carilli, C. L., & Taylor, G. B. 2002, *Annu. Rev. Astron. Astr.*, 40, 319
- Chandrasekhar, S. 1961, *Hydrodynamic and hydromagnetic stability* (Oxford Univ. Press)
- Churazov, E., Brüggen, M., Kaiser, C. R., Bohringer, H., & Forman, W. 2001, *Astrophys. J.*, 554, 261
- Del Sordo, F., Candelaresi, S., & Brandenburg, A. 2010, *Phys. Rev. E*, 81, 036401
- Dong, R., & Stone, J. M. 2009, *Astrophys. J.*, 704, 1309
- Gabuzda, D. 2018, *Galaxies*, 7, 5
- Gourgoulatos, K. N., Braithwaite, J., & Lyutikov, M. 2010, *Mon. Not. R. Astron. Soc.*, 409, 1660
- Jones, T. W., & De Young, D. S. 2005, *Astrophys. J.*, 624, 586
- Li, H., Lapenta, G., Finn, J. M., Li, S., & Colgate, S. A. 2006, *Astrophys. J.*, 643, 92
- Liu, W., Hsu, S. C., Li, H., Li, S., & Lynn, A. G. 2008, *Phys. Plasmas*, 15, 012301
- McNamara, B., & Nulsen, P. 2007, *Annu. Rev. Astron. Astr.*, 45, 117
- Montmerle, T. 2011, in *EAS Publications Series*, Vol. 51, EAS Publications Series, ed. C. Charbonnel & T. Montmerle, 299–310
- Robinson, K., et al. 2004, *Astrophys. J.*, 601, 621
- Ruszkowski, M., Enßlin, T. A., Brüggen, M., Heinz, S., & Pfrommer, C. 2007, *Mon. Not. Roy. Astron. Soc.*, 378, 662
- Sharma, R. C., & Srivastava, K. M. 1968, *Aust. J. Phys.*, 21, 917
- Su, M., Slatyer, T. R., & Finkbeiner, D. P. 2010, *Astrophys. J.*, 724, 1044
- Tang, X. Z. 2008, *Astrophys. J.*, 679, 1000
- Taylor, G. B., Fabian, A. C., & Allen, S. W. 2002, *Mon. Not. R. Astron. Soc.*, 334, 769
- Vogt, C., & Enßlin, T. A. 2005, *Astron. Astrophys.*, 434, 67
- Yang, H.-Y., Ruszkowski, M., & Zweibel, E. 2018, *Galaxies*, 6, 29